Front. Environ. Sci. Eng. 2024, 18(1): 3
https://doi.org/10.1007/s11783-024-1763-z

RESEARCH ARTICLE

# Conductive and stable polyphenylene/CNT composite membrane for electrically enhanced membrane fouling mitigation

**Huijuan Xie, Haiguang Zhang, Xu Wang, Gaoliang Wei, Shuo Chen, Xie Quan (✉)**

Key Laboratory of Industrial Ecology and Environmental Engineering (Ministry of Education), School of Environmental Science and Technology, Dalian University of Technology, Dalian 116024, China

## HIGHLIGHTS

- A conductive and stable polyphenylene/CNT membrane was fabricated.
- The conductivity of the membrane was 3.4 times higher than that of the CNT membrane.
- Structural stability of the membrane is superior to that of the CNT membrane.
- Electro-assistance can effectively enhance membrane fouling mitigation.

## GRAPHIC ABSTRACT

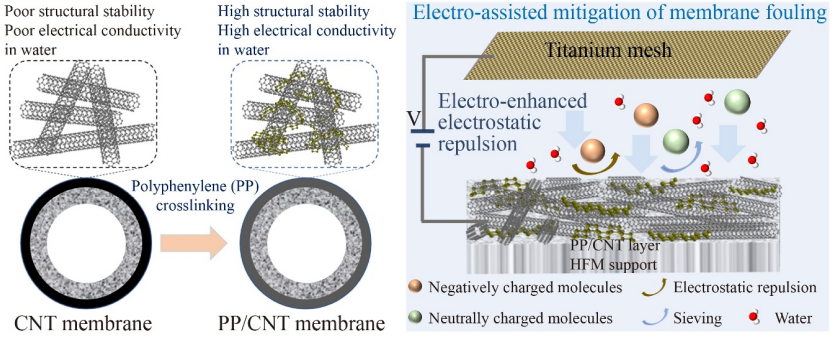


## ARTICLE INFO

*Article history:*
Received 15 March 2023
Revised 8 June 2023
Accepted 26 June 2023
Available online 15 August 2023

*Keywords:*
Polyphenylene
CNTs
Membrane
Electro-assistance
Membrane fouling mitigation

## ABSTRACT

Nanocarbon-based conductive membranes, especially carbon nanotube (CNT)-based membranes, have tremendous potential for wastewater treatment and water purification because of their excellent water permeability and selectivity, as well as their electrochemically enhanced performance (e.g., improved antifouling ability). However, it remains challenging to prepare CNT membranes with high structural stability and high electrical conductivity. In this study, a highly electroconductive and structurally stable polyphenylene/CNT (PP/CNT) composite membrane was prepared by electropolymerizing biphenyl on a CNT hollow fiber membrane. The PP/CNT membrane showed 3.4 and 5.0 times higher electrical conductivity than pure CNT and poly(vinyl alcohol)/CNT (PVA/CNT) membranes, respectively. The structural stability of the membrane was superior to that of the pure CNT membrane and comparable to that of the PVA/CNT membrane. The membrane fouling was significantly alleviated under an electrical assistance of −2.0 V, with a flux loss of only 11.7% after 5 h filtration of humic acid, which is significantly lower than those of PP/CNT membranes without electro-assistance (56.8%) and commercial polyvinylidene fluoride (PVDF) membranes (64.1%). Additionally, the rejection of negatively charged pollutants (humic acid and sodium alginate) was improved by the enhanced electrostatic repulsion. After four consecutive filtration-cleaning cycle tests, the flux recovery rate after backwashing reached 97.2%, which was much higher than those of electricity-free PP/CNT membranes (67.0%) and commercial PVDF membranes (61.1%). This study offers insights into the preparation of stable conductive membranes for membrane fouling control in potential water treatment applications.



## 1 Introduction

Membrane separation technology is widely used in water and wastewater treatment because of its high separation efficiency, low energy consumption, simple operation, and small carbon footprint (Bolisetty et al., 2019; Khanzada et al., 2020). However, membrane fouling is a primary and inevitable challenge during the membrane

✉ Corresponding author
E-mail: quanxie@dlut.edu.cn

filtration process that can reduce membrane flux, shorten membrane service life, and significantly increase processing costs (Zhang et al., 2016; Liu et al., 2022; Sutrisna et al., 2022). Alleviating membrane fouling in the filtration process effectively extends the backwash cycle of the membrane and improves membrane separation efficiency and prolongs membrane service life. In recent years, electrically conducting membranes have attracted increasing attention as promising alternatives for mitigating membrane fouling (Zhu and Jassby, 2019; Sun et al., 2021; Zhao et al., 2022). Membrane fouling, including organic fouling, inorganic fouling, and biofouling, can be effectively alleviated by various electrochemical functions such as electrostatic repulsion, electrochemical oxidation, electrolysis-induced bubble cleaning, electrophoresis, and electroosmosis (Tan et al., 2019; Li et al., 2021; Fan et al., 2023).

Currently, carbon nanomaterials (e.g., carbon nanotubes (CNTs), graphene, and carbon nanofibers) have attracted extensive attention for membrane fabrication because of their unique atomically smooth $sp^2$-carbon surfaces, delocalized π electrons, and large specific surface areas, endowing the membranes with engaging permeability, high-capacity pollutant adsorption, and high separation performance (Koros and Zhang, 2017; Alvarez et al., 2018; Patil et al., 2021; Hu et al., 2022). Among them, CNTs with excellent electrical conductivity ($10^2$–$10^6$ S/cm) are considered promising materials for preparing conductive membranes (Sears et al., 2010; Liu et al., 2020). Their one-dimensional structure is conducive to the construction of highly porous separation membranes with porosities of up to 95 ± 3% (Wei et al., 2015). In addition, the smooth and frictionless graphitised surface of CNTs can dramatically reduce water transfer resistance and achieve ultrafast water transport, with a water flow rate four to five orders of magnitude higher than that predicted by the traditional Newtonian fluid theory (Majumder et al., 2005; Holt et al., 2006). However, current conductive CNT membranes (generally prepared by the vacuum filtration method) experience poor structural stability because of the weak connections (mainly van der Waals forces) between the CNTs, which lead to instabilities in cross-flow filtration and long-term operation (Duan et al., 2016). Previous studies have shown that CNT membranes can be stabilized by chemical crosslinking using polymers such as polyvinyl alcohol and polydopamine (Soyekwo et al., 2018; Halali and de Lannoy, 2019). However, the polymers coated on the surfaces of CNTs are unfavorable for the conduction of electrons between CNTs, resulting in an increased resistance of the conductive CNT layer. Hence, it is essential to improve the structural stabilities of CNT membranes while ensuring high electrical conductivity.

Polyphenylene (PP), a typical conjugated polymer with a benzene ring chain structure, exhibits excellent conductivity (up to $10^2$ S/cm) and superior mechanical properties (Golovtsov, 2005; Bergaoui et al., 2006; Kong et al., 2023), and can be easily synthesized by electropolymerization. Moreover, its structural stability and conductivity are much higher than those of polypyrrole (PPy) and polyaniline (PANI) (Golovtsov, 2005). PP has a conjugated benzene ring chain structure with highly delocalized π electrons, exhibiting a structure similar to that of CNTs with smooth and frictionless surface properties, which is conducive to fast water transport (Li et al., 2010). In addition, PP possesses excellent material compatibility (Zhou et al., 2010; Uematsu et al., 2023), and can act as the joints of a CNT network, enhancing the binding force of the CNTs and forming a stable CNT functional layer (Martínez-Colunga et al., 2017). Based on the abovementioned features, PP could provide an opportunity to construct an electroconductive and structure-stable CNT membrane for the electro-enhanced alleviation of membrane fouling.

In this study, conductive and stable polyphenylene/CNT (PP/CNT) composite membranes were fabricated by cross-linking CNTs with conductive PP. The CNTs were vacuum-filtered onto a porous polyvinylidene fluoride (PVDF) hollow fiber (HF) membrane support to form a CNT layer and PP was then electropolymerized *in situ* on the CNT network to serve as a CNT joint. The electroconductivities and structural stabilities of the PP/CNT membranes were characterized, and pure CNT and poly(vinyl alcohol)/CNT (PVA/CNT) membranes were used for comparison. Filtration experiments of the PP/CNT membranes under different external voltages (−2.0, −1.0, 0, +1.0, and +2.0 V) were performed using humic acid (HA) as a model compound to systematically assess their antifouling abilities.

## 2 Materials and methods

### 2.1 Materials and chemicals

Carboxyl multi-walled CNTs (purity: > 95%, carboxyl: 0.49 wt%, diameter: > 50 nm) and the CNT dispersant (active substance: 90%, moisture: 10%) were supplied by Nanjing Xianfeng Nanomaterials Technology Co. Ltd., China. Sodium alginate (SA), tetrabutylammonium hexafluorophosphate ($TBAPF_6$, 98%), and biphenyl ($C_{12}H_{10}$, ⩾ 99.5%) were purchased from MacKinlin. HA was obtained from Sigma-Aldrich. Acetonitrile (ACN, ⩾ 99.9% purity) was obtained from Bengbu Paradigm Biotechnology Co., Ltd., China. Polyethylene glycol (PEG, 600 kDa) was purchased from Shanghai Eon Chemical Technology Co. Ltd., China. The commercial PVDF HF membranes (HFMs) (lined, average pore size: 0.24 μm) were obtained from Beijing BWS Water Purification Technology Co. Ltd., China.

### 2.2 Preparation of PP/CNT membranes

The preparation process of PP/CNT membranes mainly

involves the preparation of CNT membranes and the subsequent *in situ* electropolymerization of biphenyl (Fig. 1). Commercial PVDF HFMs were washed with ethanol and deionised water and then dried at room temperature (20 °C). Commercial carboxyl CNTs and a dispersant (1 g/L) were added to deionised water to form a uniform CNT dispersion (0.5 mg/mL). The as-prepared CNT dispersion was vacuum filtered using PVDF HFMs to yield CNT-PVDF membranes (CNTs loading: 0.585 mg/cm$^2$), which are denoted as CNT membranes.

PP/CNT composite membranes were prepared by the *in situ* electropolymerization of biphenyl groups on CNT membranes. Electropolymerization was conducted using a three-electrode electrochemical system. The electrolyte used for electropolymerization was an ACN solution containing biphenyl (0.1 mol/L) and $TBAPF_6$ (50 mmol/L) (Kvarnström et al., 1998; Chen et al., 2008). The electrolyte was aerated with nitrogen for 15 min before the reaction, and the polymerisation reaction was performed at a constant voltage of 3.5 V under nitrogen protection. PP/CNT membranes with various PP contents were fabricated by modulating the electropolymerization time to 10, 20, 30, 40, 50, and 60 min. The corresponding membranes are termed as $PP_x$/CNT membranes, where $x$ represents the reaction time. For comparison, PVA/CNT membranes were fabricated using a previously reported method (Wei et al., 2020), the preparation details of which can be found in Text S1.

## 2.3 Membrane characterizations

Scanning electron microscopy (SEM, S4800, Hitachi) was used to characterize the morphologies of the PP, CNT, PP/CNT membranes, and PP/CNT membranes. Fourier transform infrared spectroscopy (FTIR, VERTEX70, Bruker Optics), Raman spectroscopy (inVia Qontor, Renishaw), and X-ray photoelectron spectroscopy (XPS, 250 Xi, EscaLab) were used to analyze the components and structures of the prepared membranes. The stabilities of the CNT, PP/CNT, and PVA/CNT membranes were assessed using nanoscratch tests (UNHT, Anton Paar) and ultrasonic oscillation experiments (PS-G20, 120 W, 40 kHz, 10 min). Electrical conductivities of the CNT, PP/CNT, and PVA/CNT membranes were measured using a four-probe tester (ST-2258C). The hydrophilicities of the CNT and $PP_x$/CNT membranes were characterized using an optical contact angle meter (KINO SL 200 KB). A capillary flow porometer (POROLUX$^{TM}$1000) was used to determine the average pore sizes of the membranes, and their porosities were determined using the dry-wet weight method described in Text S2 (Wei et al., 2014). The electrochemical analysis methods for the PP/CNT membranes are presented in Text S3. A self-made dead-end filtration setup was built to measure the pure water flux (Fig. S1). In the filtration test, the quality of water permeating the membranes was analyzed after prepressurizing the membranes with pure water at 1.0 bar for 1 h. The final results were calculated using Eq. (1):

$$J = \frac{m}{\Delta P \Delta T S \rho} \times 10^{-3}, \quad (1)$$

where $J$ is the water permeance (L/(m$^2$·h·bar)), $m$ is the mass of the permeate water (g), $\Delta P$ is the transmembrane pressure (bar), $\Delta T$ is the operating time (h), $S$ is the effective membrane area (m$^2$), and $\rho$ is the water density (g/cm$^3$).

## 2.4 Antifouling tests under electro-assistance

Antifouling experiments were conducted using a custom-made electro-assisted membrane filtration device (Fig. S2). The membranes were sealed in modules with an effective filtration area of 3.14 cm$^2$. All filtration tests were conducted in the cross-flow mode, and the pressure (0.2 bar) during the filtration process was supplied by a peristaltic pump. In the electro-assisted filtration process, a cylindrical Ti mesh served as the counter electrode, and the membrane and working electrode were placed at the

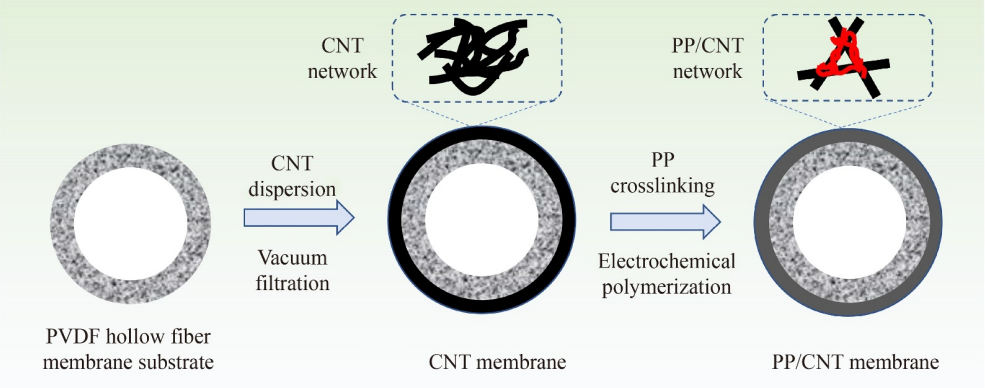


**Fig. 1** Scheme for the fabrication of PP/CNT membrane.

center of the cylindrical Ti mesh at a distance of 2 mm from the counter electrode. Considering that most natural organic matter in surface waters is negatively charged and some are neutral molecules, HA (10 mg/L) and SA (10 mg/L) were selected as negatively charged simulated pollutants, and PEG (10 mg/L) was chosen as a neutral simulated pollutant. Bacteria are also present in natural water; *Escherichia coli* (*E. coli*) was chosen as the model bacterium. The bacteria were suspended in 9 wt% NaCl solution at approximately $10^6$ colony-forming units per milliliter (cfu/mL). The antifouling performances of the membranes at different voltages for different model pollutants were investigated. The permeate flux of the membrane was calculated using Eq. (1). The fouling of the membrane with and without electro-assistance was assessed by comparing the changes in the membrane flux and flux recovery ratio (FRR). The pollutant removal ratio was calculated using Eq. (2):

$$R = \left(1 - \frac{C_P}{C_f}\right) \times 100\%, \quad (2)$$

where $R$ is the removal ratio and $C_p$ and $C_f$ are the concentrations of the permeate and feed, respectively. The HA concentration was measured at 254 nm using UV-visible spectroscopy (SP-756P). The removal ratios of SA and PEG in the membrane filtration process were determined using a total organic carbon (TOC) analyzer (TOC-VCPH, Shimadzu). Four consecutive filtration-cleaning cycle tests of the membranes were conducted to further evaluate the antifouling performance. During each cycle, HA (10 mg/L) was filtered and the fouled membrane was backwashed for 20 min at the end of the filtration.

## 3 Results and discussion

### 3.1 Characterizations of PP/CNT membrane

Photographs of the PP/CNT membranes are shown in Fig. S3. There were no obvious defects on the surfaces of the prepared membranes. The color of membrane was also observed to not significantly change after electropolymerization. The structural integrity of the membrane was further confirmed using SEM images of the membrane surface (Fig. 2). The uncrosslinked CNTs possessed smooth surfaces (Figs. 2(a) and 2(b)), which were interwoven to form a network structure. However, after the electropolymerization of PP on the CNT membrane, the morphology of the PP/CNT membrane was significantly different from that of the CNT membrane. The interwoven CNT network was more tightly connected in the crosslinked PP/CNT membrane and the joints were completely welded (Figs. 2(d) and 2(e)). With increasing electropolymerization reaction time, more PP was coated on the CNTs, increasing the crosslinking degree of the PP/CNT (Fig. S4). Fig. S5 shows the morphology of the electropolymerized PP coating. Moreover, the inner CNTs in the membrane layer were crosslinked by PP (Figs. 2(c) and 2(f)). The cross-sectional morphologies of the prepared membranes demonstrated that the thickness of the PP/CNT functional layer was approximately 4.61 μm (Fig. S6).

To prove that PP was generated by the electropolymerization of biphenyls on the CNT membrane, its chemical structure and elemental content were characterized. The FTIR spectrum is shown in Fig. 3(a), and the peak positions and corresponding attributes are listed in Table S1.

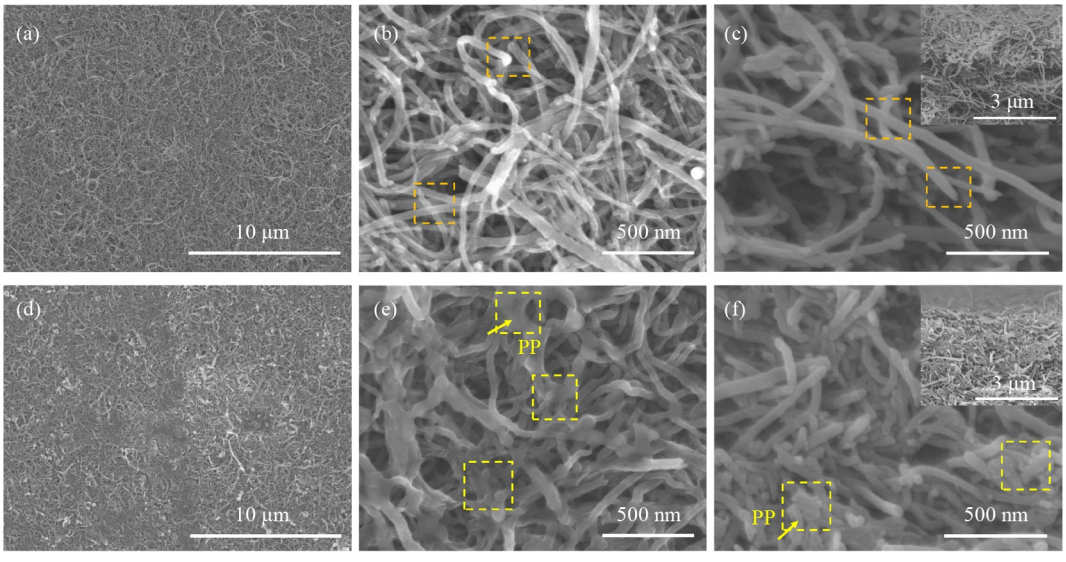


**Fig. 2** SEM images of the uncrosslinked CNT membrane of (a) surface, (b) magnified surface, and (c) cross section (inset: the low-magnification SEM image). SEM images of the crosslinked CNT membrane of (d) surface, (e) magnified surface, and (f) cross section (inset: the low-magnification SEM image).

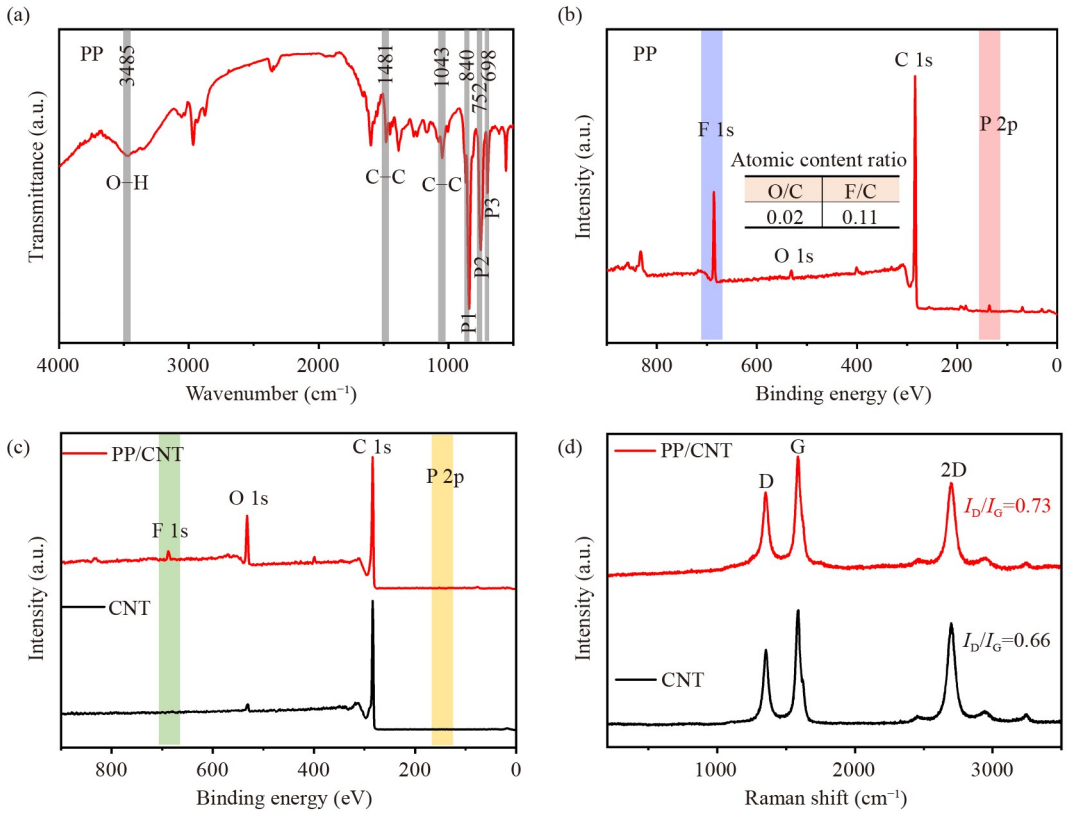


**Fig. 3** FTIR spectrum (a) and XPS spectrum (b) of PP. XPS spectra (c) and Raman spectra (d) of the CNT and PP/CNT membranes.

The peaks located at 3485, 1481, and 1043 $cm^{-1}$ correspond to O–H, C–C in the phenyl ring, and para-connected phenyl C–C stretching vibrations, respectively. Furthermore, the peak at 840 $cm^{-1}$ (P1) corresponds to C–H out-of-plane vibration of adjacent hydrogen atoms on p-disubstituted rings, and the peaks at 752 $cm^{-1}$ (P2) and 698 $cm^{-1}$ (P3) are attributed to C–H out-of-plane vibration of a mono-substituted phenyl ring (Zhou et al., 2010; Choeichom and Sirivat, 2018; Kong et al., 2023). These peaks are consistent with the characteristic peaks of PP in the range 650–900 $cm^{-1}$ reported in the literature (Castiglioni et al., 1988), which indicates that the PP is electropolymerized onto the CNT membrane (Zhou et al., 2010; Choeichom and Sirivat, 2018; Kong et al., 2023). The overall XPS spectrum (Fig. 3(b)) of PP showed multiple peaks, including F 1s, O 1s, C 1s, and P 2p. The F and P peaks are attributed to the $PF_6^-$ dopant, which is necessary for the synthesis of highly conductive PP (Chen et al., 2008; Choeichom and Sirivat, 2018). The doping content calculated from the F/C ratio reached 11.0%. Moreover, F and P peaks appeared in the XPS spectrum of PP/CNT (Fig. 3(c)). The Raman spectrum of PP/CNT is similar to that of CNTs (Fig. 3(d)), whereas the $I_D/I_G$ ratio of PP/CNT shows a slight increase compared to that of CNT, which may be attributed to the ionic dopants doped into the PP. These characterization results agree with the FTIR analysis, further confirming the successful synthesis of conductive PP on the CNT membrane.

The stabilities of the PP/CNT membranes were assessed using ultrasonic oscillation and nanoscratch tests. After ultrasonic shock treatment at 120 W for 10 min, the uncrosslinked CNT layer almost completely peeled off and re-dispersed in water (the color of the water turned black, as observed in Figs. 4(a) and 4(b)), whereas the PP/CNT membrane maintained its structural stability and no defects were visually observed on the membrane surface. In addition, the stability of the prepared PP/CNT membranes gradually increased with increasing electropolymerization reaction time (Fig. S7). The results of the nanoscratch tests are shown in Figs. 4(c) and 4(d). The non-crosslinked CNT membrane showed an obvious rupture on the surface, indicating that the applied load exceeded the critical fracture load. In contrast, the PP/CNT membrane was undamaged after the scratch test, which is similar to the test results for the PVA/CNT membrane (Fig. S8), further demonstrating the superior stability of the PP/CNT membranes. This is attributed to the tight connections formed at the joints of the CNT network by the PP coating, which possesses a $sp^2$ hybridized structure similar to those of the CNTs and can enhance the stability of the CNT network via π–π interactions.

Considering membrane filtration in aqueous solutions, it is more meaningful to measure membrane conductivity in the wet state. Fig. 4(e) exhibits the electrical conductivities of the CNT, $PP_x$/CNT, and PVA/CNT

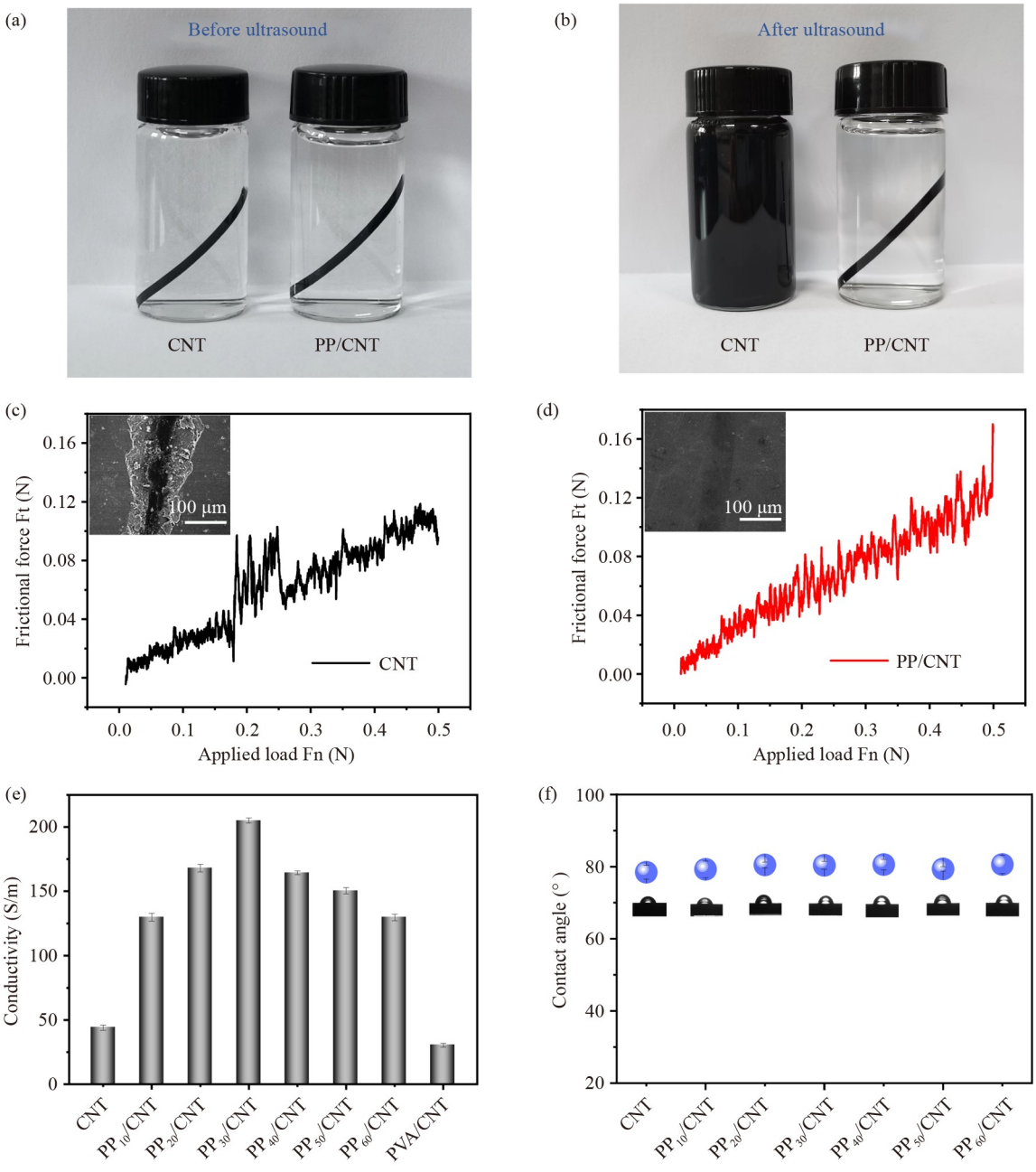


**Fig. 4** Photographs of (a) before and (b) after ultrasound of 10 min (40 kHz, 120 W) of the CNT and PP/CNT membranes. Nano-scratch results of (c) the CNT and (d) the PP/CNT membranes. Both (c) and (d) have insets showing the SEM images of nano-scratch results. (e) Conductivities of the CNT, $PP_x$/CNT and PVA/CNT membranes. (f) Water contact angles of the CNT and $PP_x$/CNT membranes.

membranes. The non-crosslinked CNT membrane can undergo swelling in water owing to the weak van der Waals forces between CNTs and the good hydrophilicity of carboxylated CNTs, leading to a decrease in electrical conductivity; and PVA is an insulating material that can increase the resistance of electron transfer in the CNT layer. In comparison, the crosslinking of PP can prevent the swelling of the CNT layer while maintaining the high conductivity of the membrane. With increasing the PP loading, the structural stability and conductivity of the PP crosslinked CNT membrane were increased. Whereas, when the electropolymerization reaction time exceeded 30 min, excess PP was coated on the CNT surface, leading to decrease conductivity of the membrane because the conductivity of PP (up to $10^2$ S/cm) is lower than that of CNTs ($10^2$ to $10^6$ S/cm), although the structural stability of the membrane improved (Fig. S7). The electrical conductivities of the structurally stable $PP_x$/CNT membranes were approximately 130–164 S/m. Those are approximately 3.0–3.7 and 4.3–5.5 times

higher than the conductivities of the uncrosslinked CNT membrane (44 S/m) and PVA/CNT membrane (30 S/m), respectively. As shown in Fig. 4(f), the water contact angles of both membranes before and after cross-linking were approximately 80°, indicating that the crosslinking of PP had a negligible impact on the hydrophilicity of the membrane. Previous studies have shown that the application of an electric potential to a conductive membrane can increase its surface hydrophilicity by inducing electrowetting (Sedev, 2011), which is beneficial for mitigating membrane fouling. Therefore, the dynamic water contact angles of PP/CNT membranes with and without electrical assistance were measured (Fig. S9). As the test time increased from 0 to 4 min, the contact angle of the membrane without electrical assistance decreased from 76.7° to 48.9°. Upon applying a voltage of −2.0 V to the membrane, the water contact angle declined from 72.3° to 45.5° within a short time of only 2 min. This result indicates that applying a negative bias to the membrane can induce electrowetting and improve the membrane hydrophilicity.

### 3.2 Performance of PP/CNT membrane

Commercial PVDF HFMs are selected as the support layer for the preparation of PP/CNT membranes, which have an average pore size of 240 nm and exhibit a water flux of 843 L/(m$^2$·h·bar). The average pore sizes and fluxes of the CNT and PP$_x$/CNT membranes are shown in Figs. 5(a) and 5(b), respectively. The flux of the CNT membrane with a pore size of 195 nm is 841 L/(m$^2$·h·bar). This flux is similar to that of the PVDF HFMs, which may be towing to the low water transport resistance originating from the randomly oriented interwoven structure of the CNT layer and smooth sp$^2$-carbon surface of the CNTs. After the PP crosslinking

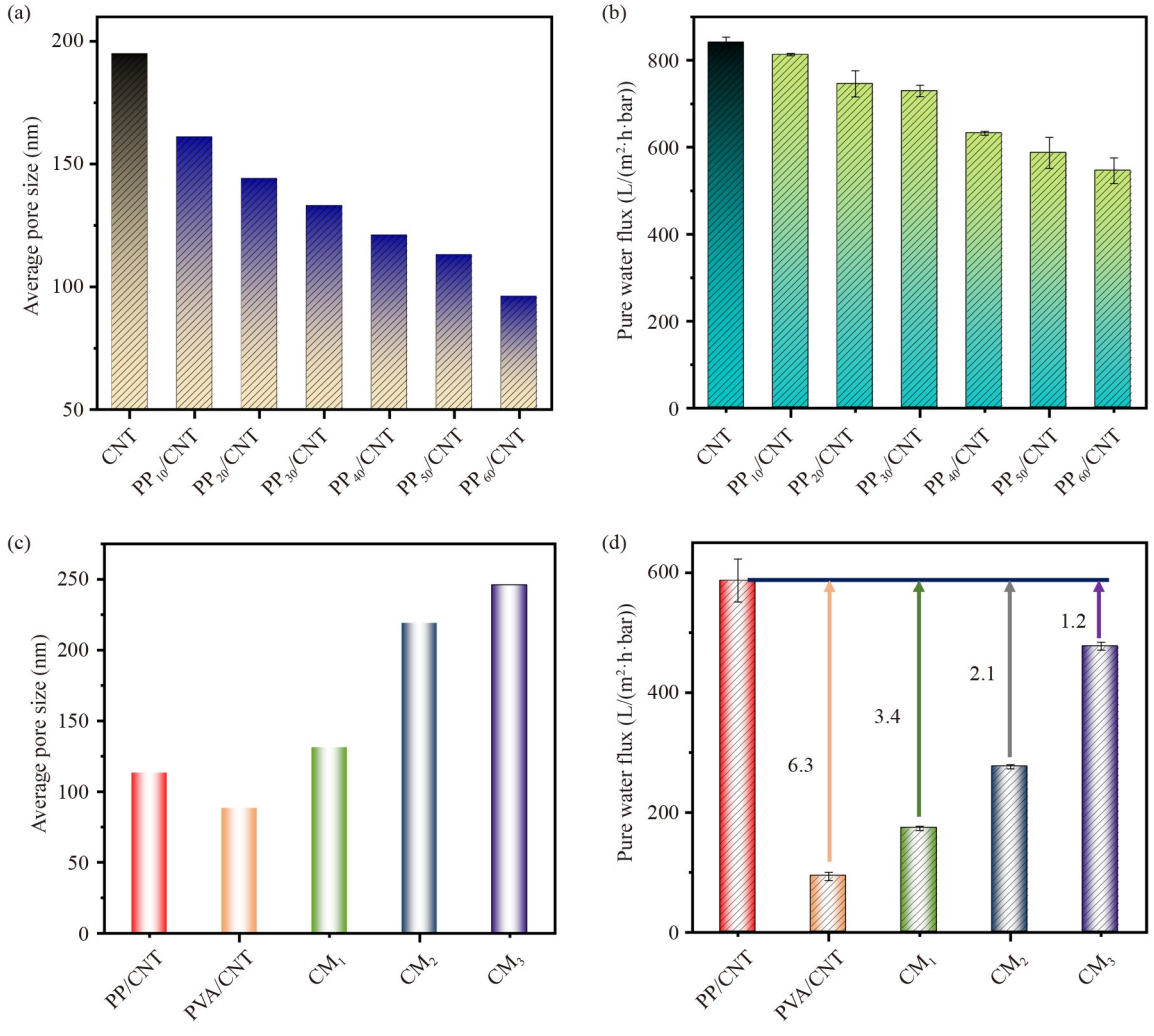


**Fig. 5** Average pore sizes (a) and pure water fluxes under operation pressure of 0.5 bar (b) of the CNT and PP$_x$/CNT membranes. Average pore sizes (c) and pure water fluxes under operation pressure of 0.5 bar (d) of the PP/CNT membrane, three commercial membranes and PVA/CNT membrane.

treatment, the pore size of the $PP_x$/CNT membranes decreased from 161 to 96 nm as the electropolymerization reaction time increased from 10 to 60 min. This is because the PP coating on the junctions of the CNT network decreased the membrane pore size. Correspondingly, the flux declined from 813 to 546 L/($m^2$·h·bar). To select the optimal membrane, the stabilities, conductivities, pore sizes and fluxes of a series of $PP_{10}$/CNT, $PP_{20}$/CNT, $PP_{30}$/CNT, $PP_{40}$/CNT, $PP_{50}$/CNT and $PP_{60}$/CNT membranes were comprehensively analyzed. Among them, $PP_{50}$/CNT and $PP_{60}$/CNT membranes have better structural stability. In particular, the $PP_{50}$/CNT membrane has a higher conductivity (150 S/m) than the $PP_{60}$/CNT membrane (130 S/m). Meanwhile, the flux of $PP_{50}$/CNT membrane (587 L/($m^2$·h·bar)) is also higher than that of the $PP_{60}$/CNT membrane (546 L/($m^2$·h·bar)). Comprehensively, the $PP_{50}$/CNT membrane exhibits superior stability, conductivity, pore size and flux. Thus, the $PP_{50}$/CNT was chosen as the optimal membrane for the subsequent investigations.

To further evaluate the permeation performance of the PP/CNT membrane, three commercial PVDF HFMs (Guangzhou Haitao Water Purification Equipment Co. Ltd. and Guangzhou Haike Filter Technology Co., Ltd., China) and a PVA/CNT membrane were selected for comparison. The three commercial PVDF HFMs are denoted as $CM_1$, $CM_2$, and $CM_3$, respectively. The PVA/CNT membrane has a pore size of 88 nm (Fig. 5(c)) and water flux of 93 L/($m^2$·h·bar) (Fig. 5(d)). The pore sizes of the $CM_1$, $CM_2$, and $CM_3$ membranes are 131, 219, and 246 nm, respectively. The corresponding water fluxes are 173, 276, and 477 L/($m^2$·h·bar). Clearly, the flux increases with pore size. In particular, the $PP_{50}$/CNT membrane exhibits a flux of 587 L/($m^2$·h·bar), which is approximately 6.3 times higher than that of the PVA/CNT membrane and 1.2–3.4 times higher than those of the three commercial $CM_1$, $CM_2$, $CM_3$ membranes with a similar or larger pore size. A possible reason for the high flux of the $PP_{50}$/CNT membrane is its high porosity. The $PP_{50}$/CNT membrane exhibited a porosity of 80 ± 3% (Table S2), which was significantly higher those that of the commercial membranes (46%–59%).

### 3.3 Antifouling performance of PP/CNT membrane

The antifouling performance of the PP/CNT membrane under electro-assistance was tested in the cross-flow mode. The PP/CNT membrane (working electrode) was placed at the center of a cylindrical Ti mesh (counter electrode) (Fig. S2(b)). Prior to the electro-assisted antifouling test, the relationship between the membrane cathode potential and the applied external voltage was investigated (Fig. S10(a)). When the applied external voltages in the system were 0, 1.0, 1.5, 2.0, and 2.5 V, the corresponding membrane cathode potentials were −0.06, −0.32, −0.44, −0.71, and −1.10 V *vs*. Ag/AgCl, respectively. In addition, the cyclic voltammetry (CV) curve of the PP/CNT membrane indicates that an electrochemical reaction occurs on the conductive membrane when the membrane cathode potential exceeds −1.1 V *vs*. Ag/AgCl (Fig. S10(b)). Such reactions may result in damage to the membrane structure and a decline in membrane performance (Zhu and Jassby, 2019). Therefore, the applied external voltage to the filtration system is set at 1.0 and 2.0 V in subsequent studies.

Considering that natural organic matter in surface waters is usually negatively charged molecules, HA with a zeta potential of approximately −19.7 mV (Wei et al., 2020), as a negatively charged model pollutants, was chosen to investigate the influence of external voltage on membrane fouling. Fig. 6(a) shows the variation in the membrane fluxes with and without electro-assistance. The flux significantly decreased in the absence of electrical assistance. After 120 min of operation, owing to membrane fouling, the flux decreased by 43.2%. In contrast, applying a negative voltage to the membrane effectively slowed the flux decline. The loss of flux was 29.8% after 120 min of operation at −1.0 V, and it further declined to only 0.8% at −2.0 V. This result indicates that increasing the negative potential of the membrane surface can enhance the electrostatic repulsion between the membrane surface and negatively charged HA, thereby improving the antifouling performance of the membrane. When the external negative voltage range was 0 to −2.0 V, the removal efficiency of HA increased from 62.5% to 87.1% (Fig. 6(b)). It was also found that if the applied voltage increased from 0 to +2.0 V, the loss of flux increased to > 50% after 120 min of operation. This is because the HA molecules are absorbed onto the membrane surface because of the electrostatic attraction between the membrane with a positive potential and the negatively charged HA, resulting in the formation of a fouling layer on the membrane surface. Compared with the membrane without electro-assistance, the removal efficiency of HA increased from 62.5% to 75.0% under the applied positive voltage from 0 to +2.0 V, which was attributed to the electro-adsorption and subsequent electrooxidation of HA (Wei et al., 2020; Fan et al., 2023). Fig. 7 shows the fouled membrane surface after HA filtration. The membrane fouling was gradually alleviated as the applied voltage changed from 0 to −2.0 V (Figs. 7(a)–7(c)) because of the electrostatic repulsion between the membrane and the negatively charged HA. In particular, there was very slight fouling on the membrane surface at a voltage of −2.0 V. Moreover, with the applied voltage increasing from 0 to +2.0 V (Figs. 7(c)–7(e)), the membrane fouling was aggravated with a dense fouling layer covering the membrane surface because of the electrostatic adsorption between the membrane with positive potential and the negatively charged HA. This suggests that applying a negative potential to the membrane can significantly

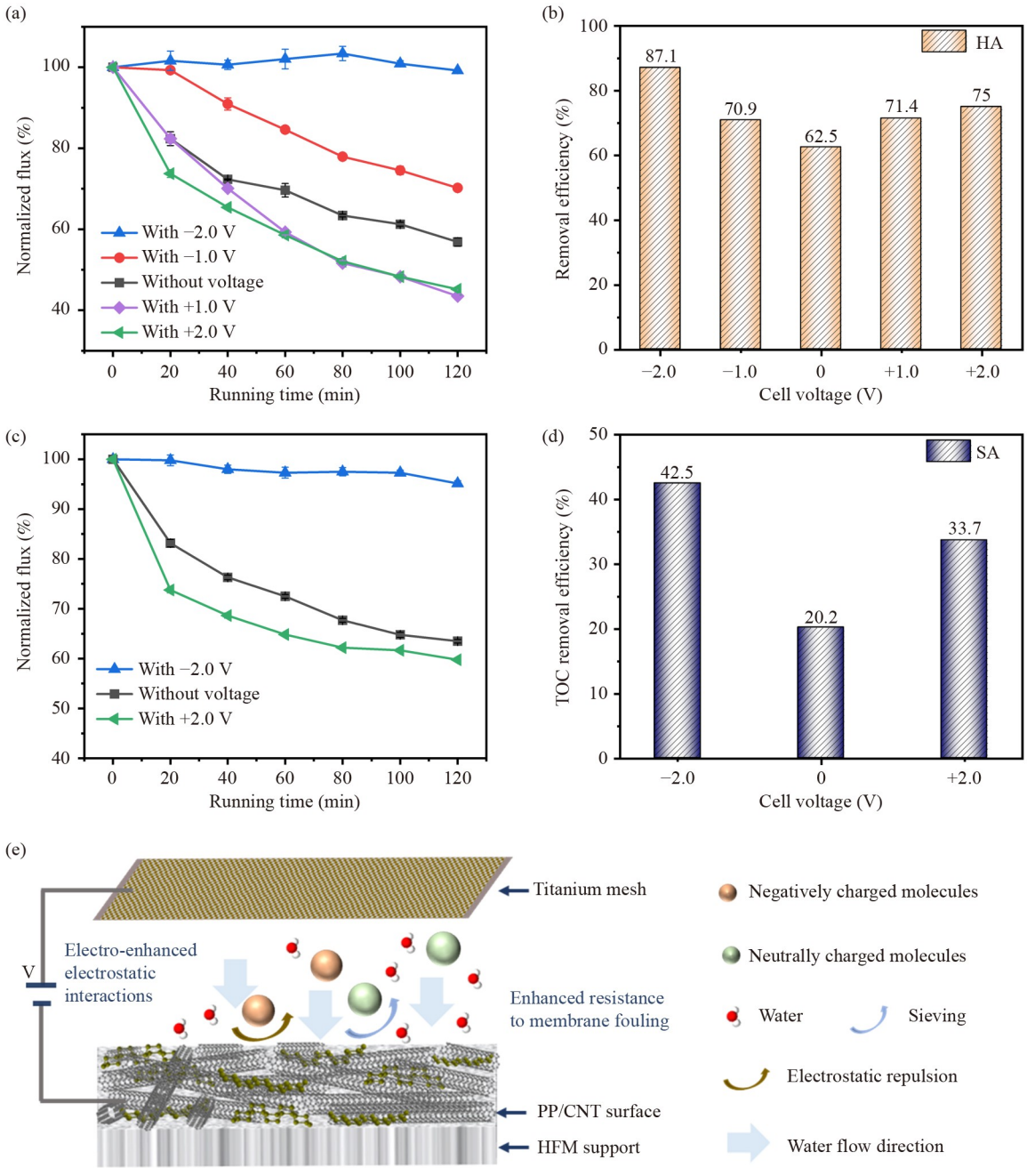


**Fig. 6** Normalized fluxes (a) and HA removal efficiency (b) of the PP/CNT membranes at different cell voltages (operation pressure of 0.2 bar). Normalized fluxes (c) and SA removal efficiency (d) of the PP/CNT membranes at different cell voltages (operation pressure of 0.2 bar). (e) Schematic diagram of the antifouling mechanism of the PP/CNT conductive membrane under electro-assistance.

alleviate the fouling caused by negatively charged pollutants.

Furthermore, another negatively charged model pollutant, SA, was selected to further study the antifouling performance of membrane. SA is a typical polysaccharide that possesses adhesive properties in water and is commonly used as a representative polysaccharide to investigate its effect on membrane fouling (Chang et al., 2016; Zhao et al., 2020). The flux variations in the PP/CNT membrane for SA filtration at different cell voltages are shown in Fig. 6(c). The permeation flux of the membrane without electro-assistance decreased by 36.5% after 120 min of operation. When a negative voltage of −2.0 V was applied to the membrane, the flux loss was only 4.9%, and fouling on the membrane surface was alleviated significantly. However, a 40.2% flux loss was observed after 120 min of operation at a voltage of +2.0 V. The fouling layer covered the entire membrane

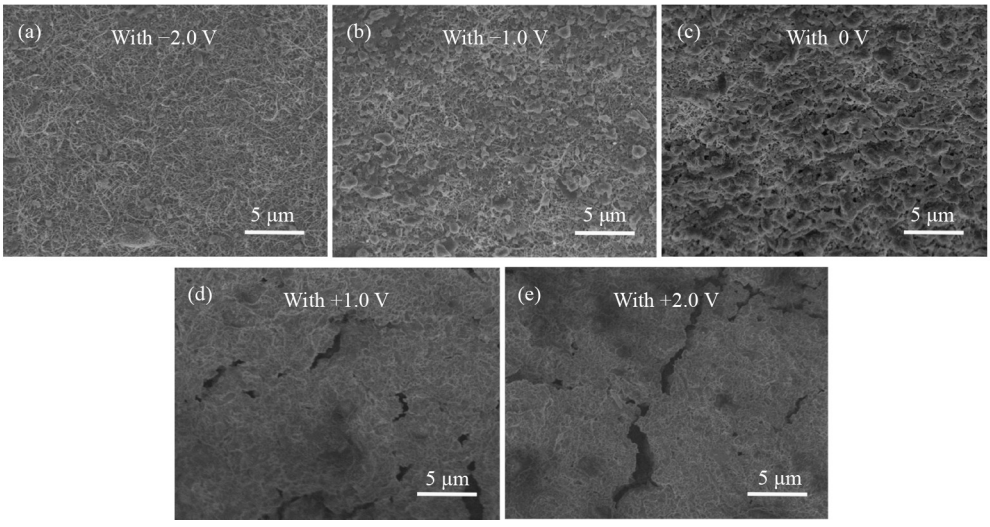


**Fig. 7** SEM images of membrane fouling of the PP/CNT membranes after HA filtration at the voltages of (a) −2.0 V, (b) −1.0 V, (c) 0 V, (d) +1.0 V, and (e) +2.0 V.

surface (Fig. S11), resulting in significant flux loss. The TOC removal efficiency of the PP/CNT membrane without electrical assistance was 20.2%, and was improved to 42.5% and 33.7% when voltages of −2.0 V and +2.0 V were applied, respectively (Fig. 6(d)). For the neutral model pollutant (PEG), negative and positive voltages improved the permeation flux and TOC removal efficiency (Figs. S12 and S13), which can be attributed to the electrically enhanced membrane hydrophilicity at negative voltages and electrooxidation of PEG at positive voltages (Fan et al., 2023).

The flux variations in the PP/CNT membranes for *E. coli* suspension filtration are shown in Fig. S14. The flux of the membrane without electro-assistance decreased by 34.3% after 120 min of operation. By contrast, the loss of flux was only 12.5% after applying a voltage of −2.0 V to the membrane, which is attributed to the enhanced electrostatic repulsion between the negatively charged bacteria and the membrane surface. In addition, the rejection rate of the PP/CNT membranes with and without electro-assistance to *E. coli* reached 100% (Fig. S15) because the size of *E. coli* is large than the membrane pore. Membrane fouling was significantly reduced by electrical assistance (Fig. S16). These results suggest that electrically assisted PP/CNT membranes can enhance anti-biofouling performance.

Based on the abovementioned results, it can be concluded that applying a negative voltage to the PP/CNT membrane is the preferred method to effectively prevent flux decline and alleviate membrane fouling using electro-enhanced hydrophilicity and electrostatic repulsion (Fig. 6(e)).

To further investigate the antifouling performance of the PP/CNT membrane, consecutive filtration-cleaning cycle tests were conducted. For comparison, a commercial PVDF HF membrane was selected. Although the pore size of $CM_1$ (average pore size: 131 nm) is closer to that of the PP/CNT membrane (average pore size: 113 nm), $CM_1$ exhibits hydrophobic properties (93°, Fig. S17), which may have exacerbated membrane fouling. In contrast, the $CM_2$ has better hydrophilicity than the $CM_1$, which means that the $CM_2$ can possess stronger antifouling performance than the $CM_1$. Therefore, we chosen the $CM_2$ (average pore size: 219 nm, contact angle: 79°) to compare the antifouling performance with the PP/CNT membrane. Fig. 8(a) shows the normalized fluxes of the PP/CNT membrane, PP/CNT membrane with −2.0 V, and $CM_2$ membrane when the HA solution was filtered. As expected, the antifouling performance of PP/CNT membrane with −2.0 V was much higher than those of the PP/CNT and $CM_2$ membranes. In the first cycle, the flux of $CM_2$ decreased by 64.1% after 5 h of operation and the flux of the PP/CNT membrane without electro-assistance decreased by 56.8%. When applying −2.0 V to the PP/CNT membrane, the flux loss was only 11.7%, suggesting that the electro-assisted membrane could significantly extend the backwashing cycle. With increasing filtration-cleaning cycles, the fluxes of the PP/CNT and $CM_2$ membranes after backwashing decreased gradually. However, the flux of PP/CNT membrane with −2.0 V was almost completely recovered after backwashing. The FRR of the membrane after hydraulic cleaning was evaluated (Fig. 8(b)). The FRR of the $CM_2$ membrane was only 61.1% after the second backwashing, and the flux decreased by 24.6% within 2 h of the third filtration, indicating that serious irreversible fouling occurred. In the photographs of the membranes (Fig. S18), severe membrane fouling is observed. Such severe fouling made it difficult to perform the fourth filtration cycle test. For the PP/CNT membrane, the FRR decreased from 87.1% to 67.0% after three hydraulic cleaning cycles, suggesting that irreversible fouling of the PP/CNT

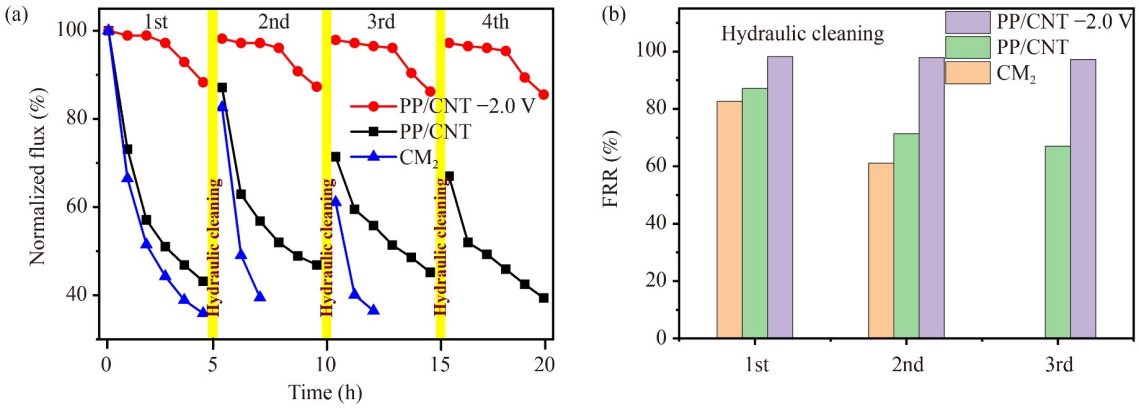


**Fig. 8** (a) Flux variations of the PP/CNT membrane, PP/CNT membrane with −2.0 V, and $CM_2$ membrane when filtrating HA solution (operation pressure of 0.2 bar). (b) Flux recovery rates (FRR) of PP/CNT membrane, PP/CNT membrane with −2.0 V, and $CM_2$ membrane after hydraulic cleaning.

membrane was lower than that of the $CM_2$ membrane. Notably, the PP/CNT membrane with −2.0 V exhibited a high FRR of 97.2% after the third (3rd) backwashing, suggesting that electro-assistance can significantly reduce irreversible fouling. Fig. S19 shows that the fouling on the membrane surface was removed by backwashing, and the pores on the membrane surface could be clearly observed. Based on these results, it can be concluded that reversible fouling mainly occurs during the initial filtration cycle, and the flux can be easily restored by hydraulic cleaning. However, the FRR gradually decreased over multiple filtration cycles because of the accumulation of irreversible fouling. When applying a negative voltage to the membrane, electro-assistance is beneficial for preventing foulants from entering the membrane pores via electrostatic repulsion between the membrane and the negatively charged foulants, inhibiting the formation of irreversible membrane fouling.

## 4 Conclusions

In this study, a conductive and stable PP/CNT composite membrane was fabricated by electropolymerizing biphenyl groups onto a CNT HF membrane. PP was coated onto the joints of the CNT network, forming a tough and integral PP/CNT functional layer that simultaneously enhanced the electroconductivity and structural stability of the membrane. The PP/CNT membrane showed an electrical conductivity of 150 S/m, which was 3.4 and 5.0 times higher than those of the CNT and PVA/CNT membranes, respectively. The structural stability was superior to that of the CNT membrane and comparable to that of the PVA/CNT membrane. It is also found that electro-assistance is an efficient strategy for alleviating irreversible membrane fouling via the electro-enhanced hydrophilicity and electrostatic repulsion between the membrane and negatively charged pollutants. The membrane fabrication and antifouling strategies proposed in this study provide new perspectives for the preparation of stable conductive membranes for membrane fouling mitigation in wastewater treatment applications.

**Acknowledgements** This work was supported by the National Key Research and Development Program of China (No. 2020YFA0211001), the National Natural Science Foundation of China (No. 22106017), the Fundamental Research Funds for the Central Universities (DUT2022TA04), and the Programme of Introducing Talents of Discipline to Universities (China) (No. B13012).

**Conflict of Interest** The authors declare that the research was conducted in the absence of any commercial or financial relationships that could be construed as a potential conflict of interest.

**Electronic Supplementary Material** Supplementary material is available in the online version of this article at https://doi.org/10.1007/s11783-024-1763-z and is accessible for authorized users.



## References

Alvarez P J J, Chan C K, Elimelech M, Halas N J, Villagran D (2018). Emerging opportunities for nanotechnology to enhance water security. Nature Nanotechnology, 13(8): 634–641

Bergaoui S, Saîd A H, Roudesli S, Matoussi F (2006). Electrosynthesis and characterization of a poly(paraphenylene) deriving from *p*-fluoroanisole. Electrochimica Acta, 51(20): 4309–4315

Bolisetty S, Peydayesh M, Mezzenga R (2019). Sustainable

technologies for water purification from heavy metals: review and analysis. Chemical Society Reviews, 48(2): 463–487

Castiglioni C, Gussoni M, Lopez Navarrete J T, Zerbi G (1988). FTIR spectra (frequency and intensity) of poly-(para-phenylenes). Mikrochimica Acta, 1(1–6): 247–249

Chang H, Liang H, Qu F, Shao S, Yu H, Liu B, Gao W, Li G (2016). Role of backwash water composition in alleviating ultrafiltration membrane fouling by sodium alginate and the effectiveness of salt backwashing. Journal of Membrane Science, 499: 429–441

Chen W, Liang C H, Yie Y, Wu B (2008). AC impedance studies on the relationship between the fractal characteristics and electrochemical properties of poly(para-phenylene) film. Journal of the Chinese Chemical Society, 55(4): 801–806

Choeichom P, Sirivat A (2018). Tuning poly(*p*-phenylene) nano-size for enhancing electrical conductivity based on surfactant templates and doping. Current Applied Physics, 18(6): 686–697

Duan W, Ronen A, Walker S, Jassby D (2016). Polyaniline-coated carbon nanotube ultrafiltration membranes: enhanced anodic stability for *in situ* cleaning and electro-oxidation processes. ACS Applied Materials & Interfaces, 8(34): 22574–22584

Fan X, Wei G, Quan X (2023). Carbon nanomaterial-based membranes for water and wastewater treatment under electrochemical assistance. Environmental Science. Nano, 10(1): 11–40

Golovtsov I (2005). Modification of Conductive Properties and Processability of Polyparaphenylene, Polypyrrole and Polyaniline. Tallinn: Tallinn University of Technology Press

Halali M A, de Lannoy C F (2019). The effect of cross-linkers on the permeability of electrically conductive membranes. Industrial & Engineering Chemistry Research, 58(9): 3832–3844

Holt J K, Park H G, Wang Y, Stadermann M, Artyukhin A B, Grigoropoulos C P, Noy A, Bakajin O (2006). Fast mass transport through sub-2-nanometer carbon nanotubes. Science, 312(5776): 1034–1037

Hu X, You S, Li F, Liu Y (2022). Recent advances in antimony removal using carbon-based nanomaterials: a review. Frontiers of Environmental Science & Engineering, 16(4): 48

Khanzada N K, Farid M U, Kharraz J A, Choi J, Tang C Y, Nghiem L D, Jang A, An A K (2020). Removal of organic micropollutants using advanced membrane-based water and wastewater treatment: a review. Journal of Membrane Science, 598: 117672

Kong W, Ge X, Yang M, Zhang Q, Lu J, Wen H, Wen H, Kong D, Zhang M, Zhu X, et al. (2023). Poly-*p*-phenylene as a novel pseudocapacitive anode or cathode material for hybrid capacitive deionization. Desalination, 553: 116452

Koros W J, Zhang C (2017). Materials for next-generation molecularly selective synthetic membranes. Nature Materials, 16(3): 289–297

Kvarnström C, Bilger R, Ivaska A, Heinze J (1998). An electrochemical quartz crystal microbalance study on polymerization of oligo-*p*-phenylenes. Electrochimica Acta, 43(3–4): 355–366

Li C, Liu M, Pschirer N G, Baumgarten M, Müllen K (2010). Polyphenylene-based materials for organic photovoltaics. Chemical Reviews, 110(11): 6817–6855

Li P, Yang C, Sun F, Li X Y (2021). Fabrication of conductive ceramic membranes for electrically assisted fouling control during membrane filtration for wastewater treatment. Chemosphere, 280: 130794

Liu X, Tian C, Zhao Y, Xu W, Dong D, Shih K, Yan T, Song W (2022). Enhanced cross-flow filtration with flat-sheet ceramic membranes by titanium-based coagulation for membrane fouling control. Frontiers of Environmental Science & Engineering, 16(8): 110

Liu Y, Gao G, Vecitis C D (2020). Prospects of an electroactive carbon nanotube membrane toward environmental applications. Accounts of Chemical Research, 53(12): 2892–2902

Majumder M, Chopra N, Andrews R, Hinds B J (2005). Enhanced flow in carbon nanotubes. Nature, 438(7064): 44

Martínez-Colunga J G, Sanchez-Valdes S, Ramos-Devalle L F, Perez-Camacho O, Ramirez-Vargas E, Benavides-Cantú R, Avila-Orta C A, Cruz-Delgado V J, Mata-Padilla J M, Lozano-Ramírez T, et al. (2018). Aniline-modified polypropylene as a compatibilizer in polypropylene carbon nanotube composites. Polymer-Plastics Technology and Engineering, 57(13): 1360–1366

Patil J J, Jana A, Getachew B A, Bergsman D S, Gariepy Z, Smith B D, Lu Z, Grossman J C (2021). Conductive carbonaceous membranes: recent progress and future opportunities. Journal of Materials Chemistry. A, Materials for Energy and Sustainability, 9(6): 3270–3289

Sears K, Dumée L, Schütz J, She M, Huynh C, Hawkins S, Duke M, Gray S (2010). Recent developments in carbon nanotube membranes for water purification and gas separation. Materials (Basel), 3(1): 127–149

Sedev R (2011). Electrowetting: electrocapillarity, saturation, and dynamics. European Physical Journal. Special Topics, 197(1): 307–319

Soyekwo F, Zhang Q, Zhen L, Ning L, Zhu A, Liu Q (2018). Borate crosslinking of polydopamine grafted carbon nanotubes membranes for protein separation. Chemical Engineering Journal, 337: 110–121

Sun M, Wang X, Winter L R, Zhao Y, Ma W, Hedtke T, Kim J H, Elimelech M (2021). Electrified membranes for water treatment applications. ACS ES&T Engineering, 1(4): 725–752

Sutrisna P D, Kurnia K A, Siagian U W R, Ismadji S, Wenten I G (2022). Membrane fouling and fouling mitigation in oil–water separation: a review. Journal of Environmental Chemical Engineering, 10(3): 107532

Tan X, Hu C, Zhu Z, Liu H, Qu J (2019). Electrically pore-size-tunable polypyrrole membrane for antifouling and selective separation. Advanced Functional Materials, 29(35): 1903081

Uematsu H, Yoshida K, Yamaguchi A, Fukushima A, Sugihara S, Yamane M, Ozaki Y, Tanoue S (2023). Enhancement of interfacial shear strength due to cooperative π−π interaction between polyphenylene sulfide and carbon fiber and molecular orientation of polyphenylene sulfide via the π−π interaction. Composites. Part A, Applied Science and Manufacturing, 165: 107355

Wei G, Chen S, Fan X, Quan X, Yu H (2015). Carbon nanotube hollow fiber membranes: high-throughput fabrication, structural control and electrochemically improved selectivity. Journal of Membrane Science, 493: 97–105

Wei G, Yu H, Quan X, Chen S, Zhao H, Fan X (2014). Constructing all carbon nanotube hollow fiber membranes with improved performance in separation and antifouling for water treatment. Environmental Science & Technology, 48(14): 8062–8068

Wei S, Du L, Chen S, Yu H, Quan X (2020). Electro-assisted

CNTs/ceramic flat sheet ultrafiltration membrane for enhanced antifouling and separation performance. Frontiers of Environmental Science & Engineering, 15: 1–11

Zhang R, Liu Y, He M, Su Y, Zhao X, Elimelech M, Jiang Z (2016). Antifouling membranes for sustainable water purification: strategies and mechanisms. Chemical Society Reviews, 45(21): 5888–5924

Zhao C, Song T, Yu Y, Qu L, Cheng J, Zhu W, Wang Q, Li P, Tang W (2020). Insight into the influence of humic acid and sodium alginate fractions on membrane fouling in coagulation-ultrafiltration combined system. Environmental Research, 191: 110228

Zhao Y, Sun M, Winter L R, Lin S, Wang Z, Crittenden J C, Ma J (2022). Emerging challenges and opportunities for electrified membranes to enhance water treatment. Environmental Science & Technology, 56(7): 3832–3835

Zhou W, Wang C, Xu J, Du Y, Yang P (2010). Enhanced electrocatalytic performance for isopropanol oxidation on Pd–Au nanoparticles dispersed on poly(*p*-phenylene) prepared from biphenyl. Materials Chemistry and Physics, 123(2–3): 390–395

Zhu X, Jassby D (2019). Electroactive membranes for water treatment: enhanced treatment functionalities, energy considerations, and future challenges. Accounts of Chemical Research, 52(5): 1177–1186